Inorganic Chemistry

Article

pubs.acs.org/IC

Tetragold(I) Complexes: Solution Isomerization and Tunable Solid-State Luminescence

Thuy Minh Dau,[†] Yi-An Chen,[‡] Antti J. Karttunen,[§] Elena V. Grachova,[⊥] Sergey P. Tunik,*[,⊥] Ke-Ting Lin,[∥] Wen-Yi Hung,[∥] Pi-Tai Chou,*[,‡] Tapani A. Pakkanen,[†] and Igor O. Koshevoy*[,†]

[†]Department of Chemistry, University of Eastern Finland, Joensuu 80101, Finland

[‡]Department of Chemistry, National Taiwan University, Taipei 106, Taiwan

[§]Department of Chemistry, Aalto University, FI-00076 Aalto, Finland

[⊥]Department of Chemistry, St. Petersburg State University, Universitetskii pr. 26, St. Petersburg 198504, Russia

[∥]Institute of Optoelectronic Sciences, National Taiwan Ocean University, Keelung 20224, Taiwan

Supporting Information

ABSTRACT: In this study, a new family of tetranuclear gold(I) triphosphine derivatives bearing alkynyl and thiolate groups have been efficiently synthesized by treating the polymeric acetylides $(AuC_2R)_n$ or a thiolate $(AuSPh)_n$ sequentially with the (a) phosphine ligand and (b) cationic complex $[Au_3(P\text{^}P\text{^}P)_2]^{3+}$ (P^P^P = $PPh_2CH_2PPhCH_2PPh_2$). The clusters $[Au_4(P\text{^}P\text{^}P)_2(C_2R)_2]^{2+}$ [R = Ph (**1**), biphenyl (**2**), terphenyl (**3**), C_6H_4OMe (**4**), $C_6H_4NMe_2$ (**5**), $C_6H_{11}O$ (**6**), and $C_6H_4CF_3$ (**7**)] and $[Au_4(P\text{^}P\text{^}P)_2(SPh)_2]^{2+}$ (**8**) were characterized by X-ray crystallography in the solid state. NMR spectroscopic investigations in solution revealed that the majority of alkynyl clusters **1**−**7** exist as two isomeric species in slow chemical equilibria. All complexes **1**−**8** exhibit moderate-to-strong photoemission in the solid state with quantum yields from 0.07 to 0.51. The luminescence behavior was rationalized using quantum chemical density functional theory methods. The high emission efficiency of these tetragold(I) compounds and their good stability in film allowed for the fabrication of an organic electroluminescent device (OLED). Employing complex **5** (Φ = 0.51), an OLED was fabricated under a solution process to give a good external quantum efficiency of 3.1%, corresponding to a current efficiency of 6.1 cd/A and a power efficiency of 5.3 lm/W, with Commission Internationale de l'Eclairage coordinates of (0.52, 0.46).

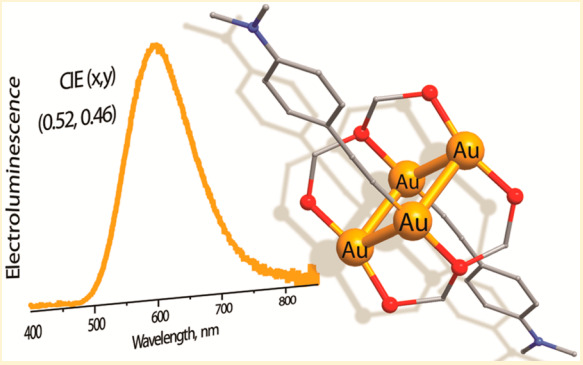

INTRODUCTION

The phenomenon of aurophilicity[1] described as weak attractive interactions between the d^{10} gold(I) ions, is a major driving force in the assembly of numerous polynuclear gold compounds with unprecedented diversity of metal frameworks.[1b,d,2] This metal−metal bonding has a strong impact on the physical characteristics of the molecules and materials, in particular leading to the appearance or variation of attractive luminescence properties found for a variety of gold-based compounds in the solid state and in solution.[2m,3] Consequently, the photophysics of gold(I) complexes turned into an active area of systematic research during the last decades. Understanding the factors that influence the excited states (i.e., emission parameters) of d^{10} luminophores requires the accumulation of a significant amount of structural and spectroscopic data and therefore stimulates considerable preparative efforts recently seen in the organometallic and inorganic chemistry of coinage metals.

In order to facilitate the formation of a Au−Au-bonded network, which is often considered to be one of the key origins of effective triplet luminescence arising from metal-centered electronic transitions,[3e−g] different types of bridging multidentate ligands have been used.[1d] Among them, oligophosphines with short bite angles, e.g., P^P, P^P^P, and P^P^P^P (^ = CH_2, $(CH_2)_2$, CH^-, NR, C═PMe_3, ferrocenyl, aromatic spacers, etc.), have been extensively employed to stabilize close Au···Au contacts and allowed for the construction of dinuclearity, trinuclearity, and higher-nuclearity compounds of gold(I).[2c,d,k,m,3b,g,4]

In a continuation of our studies on gold(I) polynuclear complexes,[2l,5] we became interested in the systematic investigation of the ligand effect on the photophysical properties of the tetragold clusters, exemplified by the triphosphine−chloride compound,[4e] Figure 1.

Since the initial report of Laguna et al., no other modifications of this framework were reported that prompted us to look for the possible variation of the ligand environment. Recently, we found a convenient route to the congener ferrocene−alkynyl tetragold clusters.[6] Herein, we present the

Received: June 20, 2014
Published: December 1, 2014

   dx.doi.org/10.1021/ic501470v | *Inorg. Chem.* 2014, 53, 12720−12731

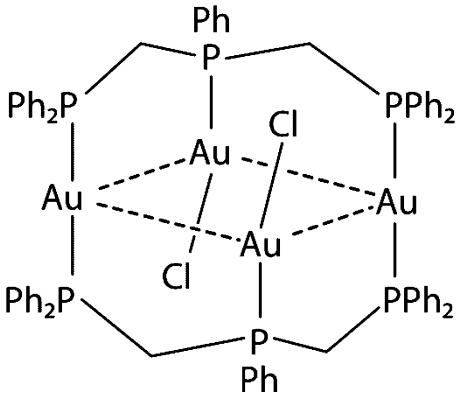

Figure 1. Schematic representation of the rhomboidal tetragold(I) triphosphine−chloride cluster.[4e]

synthesis of a family of tetranuclear gold(I) triphosphine derivatives bearing alkynyl and thiolate groups and a detailed investigation of their structures in solution and in the solid state as well as luminescent properties supported by the density functional theory (DFT) studies. From the viewpoint of practical application, we also demonstrate for the first time among polynuclear gold(I) clusters the fabrication of an organic electroluminescent device (OLED) using the tetragold(I) complex functionalized with pendant NMe_2 groups.

EXPERIMENTAL SECTION

General Comments. Bis(diphenylphosphinomethyl)-phenylphosphine (P^P^P),[7] 1-ethynylterphenyl,[8] and complexes $[Au_3(P\text{^}P\text{^}P)_2](PF_6)_3/ClO_4$,[9] $(AuC_2R)_n$ (R = Ph, biphenyl, terphenyl, 4-NMe_2-C_6H_4, 4-OMe-C_6H_4, 4-$CF_3C_6H_4$, and cyclohexanolyl)[5a,10] and $(AuSPh)_n$[11] were synthesized according to published procedures. Other reagents and solvents were used as received. The solution ^1H, $^{31}P\{^1H\}$, $^1H\{^{31}P\}$, and $^1H-^1H$ COSY NMR spectra were recorded on a Bruker Avance 400 spectrometer. Mass spectrometry (MS) spectra were determined on a Bruker micrOTOF 10223 instrument in the positive-ion electrospray ionization (ESI^+) mode. Microanalyses were carried out in the analytical laboratory of the University of Eastern Finland.

General Procedure for Preparation of the $[Au_4X_2(Ph_2PCH_2PPhCH_2PPh_2)_2](PF_6)_2$ (X = C_2R, SPh) Complexes 1−8. $(AuC_2R)_n$ or $(AuSPh)_n$ (0.15 mmol) and P^P^P (28 mg; 0.055 mmol) were suspended in CH_2Cl_2 (10 cm^3). The reaction mixture was stirred for 30 min to give a transparent, nearly colorless solution. Then $[Au_3(P\text{^}P\text{^}P)_2](PF_6)_3$ (102 mg, 0.05 mmol) was added, and the reaction mixture was stirred for 30 min. The solvent was evaporated, and the solid residue was recrystallized.

*$[Au_4(C_2Ph)_2(Ph_2PCH_2PPhCH_2PPh_2)_2](PF_6)_2$ (**1**).* **1** was recrystallized by gas-phase diffusion of diethyl ether into an acetone solution at 278 K to give a colorless crystalline material (145 mg, 84%). ESI MS: *m*/*z* 1001.12 (calcd 1001.12; $[M]^{2+}$). $^{31}P\{^1H\}$ NMR (DMSO-d_6, 298 K; δ): form **I**, A_4B_2 system, J_{AA} = 320 Hz, J_{AB} = 76 Hz, 41.1 (m, 4P, **A**), 24.4 (m, 2P, **B**), −144.2 (sept, 2P, PF_6^-); form **II**, 31.6 (m br, 4P, **A**), 26.2 (m br, 2P, **B**), −144.2 (sept, 2P, PF_6^-); the ratio of form **I**/form **II** is ca. 4:3 at equilibrium. $^{31}P\{^1H\}$ NMR (acetone-d_6, 298 K; δ): form **I**, A_4B_2 system, J_{AA} = 320 Hz, J_{AB} = 76 Hz, 40.0 (m, 4P, **A**), 22.1 (m, 2P, **B**), −144.8 (sept, 2P, PF_6^-); form **II**, A_4B_2 system, J_{AA} = 320 Hz, J_{BB} = 320 Hz, J_{AB} = 60 Hz, 30.8 (m, 4P, **A**), 25.1 (m, 2P, **B**), −144.8 (sept, 2P, PF_6^-); the ratio of form **I**/form **II** is ca. 5:1 at equilibrium. $^{31}P\{^1H\}$ NMR (CD_2Cl_2, 298 K; δ): form **I**, A_4B_2 system, J_{AA} = 318 Hz, J_{AB} = 76 Hz, 40.1 (m, 4P, **A**), 21.5 (m, 2P, **B**), −143.9 (sept, 2P, PF_6^-); form **II**, 31.6 (m, 4P, **A**), 25.6 (m, 2P, **B**), −143.9 (sept, 2P, PF_6^-); the ratio of form **I**/form **II** is ca. 3:1 at equilibrium. ^1H NMR (acetone-d_6, 298 K; δ): 7.88 (m, 8H, J_{HH} = 7.7 Hz, J_{PH} = 14.0 Hz, *o*-H, phosphine Ph[a]), 7.72 (m, 8H, J_{HH} = 7.4 Hz, J_{PH} = 13.8 Hz, *o*-H, phosphine Ph[b]), 7.66 (m, 12H, AB_2 system of *m*-H + *p*-H, phosphine Ph[a]), 7.52 (m, 4H, J_{HH} = 7.4 Hz, J_{PH} = 13.5 Hz, Hz, *o*-H, phosphine Ph[c]), 7.52−7.44 (unresolved multiplet, 10H, *o*-H + *m*-H + *p*-H, alkynyl ligand), 7.43 (t, 2H, J_{HH} = 7.4 Hz, *p*-H, phosphine Ph[c]), 7.42 (t, 4H, J_{HH} = 7.4 Hz, *p*-H, phosphine Ph[b]), 7.20 (dd, 8H, J_{HH} = 7.4 Hz, *m*-H, phosphine Ph[b]), 7.17 (dd, 4H, J_{HH} = 7.4 Hz, *m*-H, phosphine Ph[c]), 5.22 (m, 8H, CH_2, phosphine), 5.09 (m, 8H, CH_2, phosphine). Anal. Calcd for $Au_4C_{80}H_{68}P_8F_{12}$: C, 41.90; H, 2.99. Found: C, 41.94; H, 2.99.

*$[Au_4(C_2C_6H_4Ph)_2(Ph_2PCH_2PPhCH_2PPh_2)_2](PF_6)_2$ (**2**).* **2** was recrystallized by gas-phase diffusion of diethyl ether into an acetone/methanol [3:1 (v/v)] solution at 278 K to give a light-yellow crystalline material (165 mg, 90%). ESI MS: *m*/*z* 1077.15 (calcd 1077.15; $[M]^{2+}$). $^{31}P\{^1H\}$ NMR (DMSO-d_6, 298 K; δ): form **I**, A_4B_2 system, J_{AA} = 320 Hz, J_{AB} = 77 Hz, 41.1 (m, 4P, **A**), 24.4 (m, 2P, **B**), −144.2 (sept, 2P, PF_6^-); form **II**, 31.6 (m, 4P, **A**), 26.1 (m, 2P, **B**), −144.2 (sept, 2P, PF_6^-); the ratio of form **I**/form **II** is ca. 7:10 at equilibrium. ^1H NMR (DMSO-d_6, 298 K; δ): form **I**, 7.91 (m, 8H, J_{HH} = 7.7 Hz, J_{PH} = 12.5 Hz, *o*-H, phosphine Ph[a]), 7.73 (d, 4H, J_{HH} = 7.7 Hz, *o*-H, C_6H_5, alkynyl ligand), 7.70 (m, 12H, AB_2 system of *m*-H + *p*-H, phosphine Ph[a]), 7.68 (d, 4H, J_{HH} = 8.2 Hz, C_6H_4, alkynyl ligand), 7.63 (m, 8H, J_{HH} = 7.3 Hz, J_{PH} = 13.7 Hz, *o*-H, phosphine Ph[b]), 7.54 (dd, 4H, J_{HH} = 7.7 Hz, *m*-H, C_6H_5, alkynyl ligand), 7.47 (m, 4H, J_{HH} = 7.3 Hz, J_{PH} = 13.9 Hz, *o*-H, phosphine Ph[c]), 7.44 (t, 2H, J_{HH} = 7.7 Hz, *p*-H, C_6H_5, alkynyl ligand), 7.39 (t, 4H, J_{HH} = 7.3 Hz, *p*-H, phosphine Ph[b]), 7.39 (t, 2H, J_{HH} = 7.3 Hz, *p*-H, phosphine Ph[c]), 7.29 (d, 4H, J_{HH} = 8.2 Hz, C_6H_4, alkynyl ligand), 7.16 (dd, 8H, J_{HH} = 7.3 Hz, *m*-H, phosphine Ph[b]), 7.11 (dd, 4H, J_{HH} = 7.3 Hz, *m*-H, phosphine Ph[c]), 5.50 (m, 4H, CH_2, phosphine), 4.60 (m, 4H, CH_2, phosphine). Anal. Calcd for $Au_4C_{92}H_{76}P_8F_{12}$: C, 45.19; H, 3.13. Found: C, 45.21; H, 3.12.

*$[Au_4(C_2(C_6H_4)_2Ph)_2(Ph_2PCH_2PPhCH_2PPh_2)_2](PF_6)_2$ (**3**).* **3** was recrystallized by gas-phase diffusion of diethyl ether into an acetone/methanol [3:1 (v/v)] solution at 278 K to give a light-yellow crystalline material (173 mg, 89%). ESI MS: *m*/*z* 1153.18 (calcd 1153.18; $[M]^{2+}$). $^{31}P\{^1H\}$ NMR (DMSO-d_6, 298 K; δ): form **I**, A_4B_2 system, J_{AA} = 320 Hz, J_{AB} = 73 Hz, 41.1 (m, 4P, **A**), 24.4 (m, 2P, **B**), −144.2 (sept, 2P, PF_6^-); form **II**, 31.6 (m, 4P), 26.2 (m, 2P), −144.2 (sept, 2P, PF_6^-); the ratio of form **I**/form **II** is ca. 3:5 at equilibrium. ^1H NMR (DMSO-d_6, 298 K; δ): form **I**, 7.92 (m, 8H, J_{HH} = 7.7 Hz, J_{PH} = 14.5 Hz, *o*-H, phosphine Ph[a]), 7.84 (s, 8H, C_6H_4, alkynyl ligand), 7.77 (d, 4H, J_{HH} = 7.2 Hz, *o*-H, C_6H_5, alkynyl ligand), 7.75 (d, 4H, J_{HH} = 8.7 Hz, C_6H_4, alkynyl ligand), 7.73 (m, 12H, AB_2 system of *m*-H + *p*-H, phosphine Ph[a]), 7.64 (m, 8H, J_{HH} = 7.5 Hz, J_{PH} = 14.2 Hz, *o*-H, phosphine Ph[b]), 7.53 (dd, 4H, J_{HH} = 7.2 Hz, *m*-H, C_6H_5, alkynyl ligand), 7.46 (m, 4H, J_{HH} = 7.8 Hz, J_{PH} = 14.2 Hz, *o*-H, phosphine Ph[c]), 7.43 (t, 2H, J_{HH} = 7.2 Hz, *p*-H, C_6H_5, alkynyl ligand), 7.40 (t, 4H, J_{HH} = 7.5 Hz, *p*-H, phosphine Ph[b]), 7.40 (t, 2H, J_{HH} = 7.8 Hz, *p*-H, phosphine Ph[c]), 7.32 (d, 4H, J_{HH} = 8.7 Hz, C_6H_4, alkynyl ligand), 7.17 (dd, 8H, J_{HH} = 7.5 Hz, *m*-H, phosphine Ph[b]), 7.12 (dd, 4H, J_{HH} = 7.8 Hz, *m*-H, phosphine Ph[c]), 5.51 (m, 4H, CH_2, phosphine), 4.61 (m, 4H, CH_2, phosphine). Anal. Calcd for $Au_4C_{104}H_{84}P_8F_{12}$: C, 48.09; H, 3.26. Found: C, 47.91; H, 3.28.

*$[Au_4(C_2C_6H_4OMe)_2(Ph_2PCH_2PPhCH_2PPh_2)_2](PF_6)_2$ (**4**).* **4** was recrystallized by gas-phase diffusion of diethyl ether into an acetone solution at 278 K to give a light-yellow crystalline material (155 mg, 88%). ESI MS: *m*/*z* 1031.13 (calcd 1031.13; $[M]^{2+}$). $^{31}P\{^1H\}$ NMR (acetone-d_6, 298 K; δ): form **I**, A_4B_2 system, J_{AA} = 320 Hz, J_{AB} = 76 Hz, 40.0 (m, 4P, **A**), 22.2 (m, 2P, **B**), −144.8 (sept, 2P, PF_6^-); form **II**, 30.9 (m, 4P, **A**), 25.1 (m, 2P, **B**), −144.8 (sept, 2P, PF_6^-); the ratio of form **I**/form **II** is ca. 4:1 at equilibrium. ^1H NMR (acetone-d_6, 298 K; δ): form **I**, 7.88 (m, 8H, J_{HH} = 7.1 Hz, J_{PH} = 14.8 Hz, *o*-H, phosphine Ph[a]), 7.71 (m, 8H, J_{HH} = 7.8 Hz, J_{PH} = 14.2 Hz, *o*-H, phosphine Ph[b]), 7.67 (m, 12H, AB_2 system of *m*-H + *p*-H, phosphine Ph[a]), 7.52 (m, 4H, J_{HH} = 7.8 Hz, J_{PH} = 14.0 Hz, Hz, *o*-H, phosphine Ph[c]), 7.42 (t, 4H, J_{HH} = 7.8 Hz, *p*-H, phosphine Ph[b]), 7.41 (t, 2H, J_{HH} = 7.8 Hz, *p*-H, phosphine Ph[c]), 7.41 (d, 4H, J_{HH} = 8.4 Hz, C_6H_4, alkynyl ligand), 7.19 (dd, 8H, J_{HH} = 7.8 Hz, *m*-H, phosphine Ph[b]), 7.17 (dd, 4H, J_{HH} = 7.8 Hz, *m*-H, phosphine Ph[c]), 6.98 (d, 4H, J_{HH} = 8.4 Hz, C_6H_4, alkynyl ligand), 5.14 (m, 8H, CH_2, phosphine), 3.89 (s, 6H, CH_3, alkynyl ligand). Anal. Calcd for $Au_4C_{82}H_{72}P_8O_2F_{12}$: C, 41.85; H, 3.08. Found: C, 41.89; H, 3.08.

dx.doi.org/10.1021/ic501470v | *Inorg. Chem.* 2014, 53, 12720−12731

[Au$_4$(C$_2$C$_6$H$_4$NMe$_2$)$_2$(Ph$_2$PCH$_2$PPhCH$_2$PPh$_2$)$_2$](PF$_6$)$_2$ (**5**). **5** was recrystallized by gas-phase diffusion of diethyl ether into a dichloromethane/methanol [1:1 (v/v)] solution at 278 K to give a bright-yellow crystalline material (155 mg, 87%). ESI MS: *m*/*z* 1044.16 (calcd 1044.16; [M]$^{2+}$). ^{31}P{^{1}H} NMR (acetone-*d*$_6$, 298 K; *δ*): A$_4$B$_2$ system, J_{AA} = 320 Hz, J_{AB} = 77 Hz, 40.0 (m, 4P, **A**), 22.4 (m, 2P, **B**), −144.8 (sept, 2P, PF$_6^-$). ^{1}H NMR (acetone-*d*$_6$, 298 K; *δ*): 7.87 (m, 8H, J_{HH} = 7.4 Hz, J_{PH} = 14.0 Hz, *o*-H, phosphine Ph^a), 7.71 (m, 8H, J_{HH} = 7.7 Hz, J_{PH} = 14.8 Hz, *o*-H, phosphine Ph^b), 7.68 (m, 12H, AB$_2$ system of *m*-H + *p*-H, phosphine Ph^a), 7.51 (m, 4H, J_{HH} = 7.6 Hz, J_{PH} = 13.9 Hz, Hz, *o*-H, phosphine Ph^c), 7.42 (t, 2H, J_{HH} = 7.7 Hz, *p*-H, phosphine Ph^c), 7.42 (t, 4H, J_{HH} = 7.7 Hz, *p*-H, phosphine Ph^b), 7.31 (d, 4H, J_{HH} = 8.7 Hz, alkynyl ligand), 7.19 (dd, 4H, J_{HH} = 7.7 Hz, *m*-H, phosphine Ph^c), 7.19 (dd, 8H, J_{HH} = 7.7 Hz, *m*-H, phosphine Ph^b), 6.74 (d, 4H, J_{HH} = 8.7 Hz, alkynyl ligand), 5.13 (m, 8H, CH$_2$, phosphine), 3.06 (s, 12H, CH$_3$, alkynyl ligand). Anal. Calcd for Au$_4$C$_{84}$H$_{78}$P$_8$N$_2$F$_{12}$: C, 42.41; H, 3.30. Found: C, 42.26; H, 3.40.

[Au$_4$(C$_2$C$_6$H$_{11}$O)$_2$(Ph$_2$PCH$_2$PPhCH$_2$PPh$_2$)$_2$](ClO$_4$)$_2$ (**6**). **6** was recrystallized by gas-phase diffusion of diethyl ether into an acetone solution at 278 K to give a colorless crystalline material (133 mg, 79%). ESI MS: *m*/*z* 1023.17 (calcd 1023.16; [M]$^{2+}$). ^{31}P{^{1}H} NMR (acetone-*d*$_6$, 298 K; *δ*): A$_4$B$_2$ system, J_{AA} = 318 Hz, J_{AB} = 78 Hz, 39.8 (m, 4P, **A**), 22.0 (m, 2P, **B**). ^{1}H NMR (acetone-*d*$_6$, 298 K; *δ*): 7.96 (m, 8H, J_{HH} = 7.2 Hz, J_{PH} = 12.6 Hz, *o*-H, phosphine Ph^a),7.68 (m, 8H, J_{HH} = 7.2 Hz, J_{PH} = 13.7 Hz, *o*-H, phosphine Ph^b), 7.64 (m, 12H, AB$_2$ system of *m*-H + *p*-H, phosphine Ph^a), 7.47 (m, 4H, J_{HH} = 7.7 Hz, J_{PH} = 13.5 Hz, Hz, *o*-H, phosphine Ph^c), 7.40 (t, 2H, J_{HH} = 7.3 Hz, *p*-H, phosphine Ph^c), 7.40 (t, 4H, J_{HH} = 7.3 Hz, *p*-H, phosphine Ph^b), 7.12 (dd, 4H, J_{HH} = 7.3 Hz, *m*-H, phosphine Ph^c), 7.12 (dd, 8H, J_{HH} = 7.3 Hz, *m*-H, phosphine Ph^b), 5.50 (m, 4H, CH$_2$, phosphine), 5.00 (m, 4H, CH$_2$, phosphine), 4.49 (s, 2H, OH, alkynyl ligand), 1.73 (m, 10H, CH$_2$, alkynyl ligand). Anal. Calcd for Au$_4$C$_{80}$H$_{80}$P$_6$Cl$_2$O$_{10}$: C, 42.78; H, 3.59. Found: C, 42.79; H, 3.73.

[Au$_4$(C$_2$C$_6$H$_4$CF$_3$)$_2$(Ph$_2$PCH$_2$PPhCH$_2$PPh$_2$)$_2$](PF$_6$)$_2$ (**7**). **7** was recrystallized by the slow evaporation of an acetone/isopropyl alcohol solution at 278 K to give a light-yellow crystalline material (151 mg, 83%). ESI MS: *m*/*z* 1069.11 (calcd 1069.11; [M]$^{2+}$). ^{31}P{^{1}H} NMR (acetone-*d*$_6$, 298 K; *δ*): form **I**, A$_4$B$_2$ system, J_{AA} = 320 Hz, J_{AB} = 75 Hz, 41.8 (m, 4P, **A**), 23.7 (m, 2P, **B**), −144.8 (sept, 2P, PF$_6^-$); form **II**, A$_4$B$_2$ system, J_{AA} = 310 Hz, J_{BB} = 310 Hz, J_{AB} = 74 Hz, 31.0 (m, 4P, **A**), 25.6 (m, 2P, **B**), −144.8 (sept, 2P, PF$_6^-$). ^{1}H NMR (acetone-*d*$_6$, 298 K; *δ*): 7.81 (m, 8H, J_{HH} = 7.0 Hz, J_{PH} = 13.2 Hz, *o*-H, phosphine Ph^a), 7.76 (m, 8H, J_{HH} = 7.1 Hz, J_{PH} = 13.2 Hz, *o*-H, phosphine Ph^b), 7.64 (m, 4H, J_{HH} = 7.4 Hz, J_{PH} = 14.0 Hz, *o*-H, phosphine Ph^c), 7.42 (t, 4H, J_{HH} = 7.1 Hz, *p*-H, phosphine Ph^b), 7.40 (m, 12H, AB$_2$ system of *m*-H + *p*-H, phosphine Ph^a), 7.37 (t, 2H, J_{HH} = 7.4 Hz, *p*-H, phosphine Ph^c), 7.25 (dd, 8H, J_{HH} = 7.1 Hz, *m*-H, phosphine Ph^b), 7.18 (dd, 4H, J_{HH} = 7.4 Hz, *m*-H, phosphine Ph^c), 7.06 (d, 4H, J_{HH} = 8.1 Hz, C$_6$H$_4$, alkynyl ligand), 6.69 (d, 4H, J_{HH} = 8.1 Hz, C$_6$H$_4$, alkynyl ligand), 5.36 (m, 4H, CH$_2$, phosphine), 4.64 (m, 4H, CH$_2$, phosphine). Anal. Calcd for Au$_4$C$_{82}$H$_{66}$P$_8$F$_{18}$: C, 40.55; H, 2.74. Found: C, 40.48; H, 2.76.

[Au$_4$(SPh)$_2$(Ph$_2$PCH$_2$PPhCH$_2$PPh$_2$)$_2$](PF$_6$)$_2$ (**8**). **8** was recrystallized by the slow evaporation of an acetone/isopropyl alcohol solution at 278 K to give a yellow crystalline material (152 mg, 88%). ESI MS: *m*/*z* 1009.09 (calcd 1009.09; [M]$^{2+}$). ^{31}P{^{1}H} NMR (DMSO-*d*$_6$, 298 K; *δ*): A$_4$B$_2$ system, J_{AA} = 320 Hz, J_{AB} = 82 Hz, 42.3 (m, 4P, **A**), 26.5 (m, 2P, **B**), −144.2 (sept, 2P, PF$_6^-$). ^{1}H NMR (DMSO-*d*$_6$, 298 K; *δ*): 7.90 (m, 8H, J_{HH} = 7.2 Hz, J_{PH} = 13.4 Hz, *o*-H, phosphine Ph^a), 7.63 (m, 12H, J_{HH} = ∼7.5 Hz, AB$_2$ system of *m*-H + *p*-H, phosphine Ph^a), 7.51 (m, 8H, J_{HH} = 7.2 Hz, J_{PH} = 13.4 Hz, *o*-H, phosphine Ph^b), 7.32 (m, 4H, J_{HH} = 7.5 Hz, J_{PH} = Hz, *o*-H, phosphine Ph^c), 7.30 (t, 4H, J_{HH} = 7.2 Hz, *p*-H, phosphine Ph^b), 7.16−7.09 (unresolved multiplet, 10H, *o*-H + *m*-H + *p*-H, SPh), 7.14 (t, 2H, J_{HH} = 7.5 Hz, *p*-H, phosphine Ph^c), 6.97 (dd, 8H, J_{HH} = 7.2 Hz, *m*-H, phosphine Ph^b), 6.96 (dd, 4H, J_{HH} = 7.5 Hz, *m*-H, phosphine Ph^c), 5.34 (m, 8H, CH$_2$, phosphine), 4.61 (m, 8H, CH$_2$, phosphine). Anal. Calcd for Au$_4$C$_{76}$H$_{68}$P$_8$S$_2$F$_{12}$: C, 39.53; H, 2.97; S, 2.78. Found: C, 39.51; H, 2.98; S, 2.61.

X-ray Structure Determination. The crystals of **1**−**8** were immersed in cryo-oil, mounted in a Nylon loop, and measured at a temperature of 120 K. The X-ray diffraction (XRD) data were collected on a Bruker SMART APEX II diffractometer using Mo K*α* radiation (*λ* = 0.71073 Å). The *APEX2*[12] program package was used for cell refinement and data reduction. The structures were solved by direct methods using the *SHELXS-97*[13] programs with the *WinGX*[14] graphical user interface. A semiempirical absorption correction (*SADABS*)[15] was applied to all data. Structural refinements were carried out using *SHELXL-97*.[13] The displacement parameters of the carbon atoms of the diethyl ether crystallization molecule in **1** were constrained to be equal. The crystallization acetone in **2** and methanol in **5** were partially lost. Acetone solvent and methanol in **3** and **5**, respectively, were disordered over two equivalent positions; therefore, these moieties were refined with an occupancy of 0.5. Both geometrical and displacement constraints and restraints were applied to these molecules. The displacement parameters of the C(34) and C(35) atoms of one phenyl ring in **7** were restrained so that their U_{ij} components approximate to isotropic behavior. The displacement parameters of the atoms C(30)−C(35) in the phenyl ring and of the carbon atoms in the acetone crystallization molecule were constrained to be equal within each moiety. Some of the solvent was lost from the crystal of **7** and could not been resolved unambiguously. The missing solvent was taken into account by using a *SQUEEZE* routine of *PLATON*.[16] The contribution of the missing solvent was not taken into account in the unit cell content. All hydrogen atoms in **1**−**8** were positioned geometrically and constrained to ride on their parent atoms, with O−H = 0.84 Å, C−H = 0.95−0.99 Å, and U_{iso} = 1.2−1.5U_{eq} (parent atom). The crystallographic details are summarized in Table S1 in the Supporting Information (SI).

Photophysical Measurements. The steady-state absorption and emission measurements in solution were recorded on a Hitachi (U-3310) spectrophotometer and an Edinburgh (FS920) fluorometer. Both the wavelength-dependent excitation and emission responses of the fluorometer have been calibrated. The samples were dissolved in dichloromethane, which was used as received. To determine the photoluminescence (PL) quantum yield in solution, the samples were degassed by three freeze−pump−thaw cycles. Coumarin 480 in methanol with a quantum yield of 0.87[17] served as the standard for measuring the quantum yields of the samples.[18] Nanosecond lifetime studies were performed with an Edinburgh FL 900 photon-counting system using a hydrogen-filled lamp as the excitation source. The emission decays were fitted by the sum of the exponential functions with a temporal resolution of ∼300 ps via deconvolution of the instrument response function. The lifetime fitting equation $R(t) = A + B_1e^{(-t/\tau_1)}$. *A* is a constant background, B_1 is the preexponential factor, and τ_1 is the lifetime. We used an integrating sphere (Horiba Quanta-*φ*) to measure the emission quantum yield of the solids. The uncertainty of the quantum yield measurement was in the range of ±5% (an average of three replicas, which correspond to different orientations of a sample). The integrating sphere consists of a 120-mm-inside-diameter spherical cavity, surrounded by an aluminum shell for handling and protection. This integrating sphere has two perpendicular ports, one with a lens to focus the excitation beam into the sample and a window to collect a portion of the light scattered off the sphere's surface. The integrating sphere fits directly in the sample chamber in place of the regular sample holder and allows measurement of the fluorescence quantum yield by an absolute method.[19] No neutral density filter was used for these measurements. The experimental highest occupied molecular orbital (HOMO) energy levels were determined by atmospheric ultraviolet photoelectron spectroscopy (Rikken Keiki AC-2); the lowest unoccupied molecular orbital (LUMO) energy levels were estimated by the equation of LUMO = HOMO + E_g (where E_g is the optical band gap determined from the absorption threshold).

Device Fabrication and Measurements. Because of the nonvolatility of the title tetragold complexes, the fabrication of an OLED using a vapor deposition process is not feasible. Instead, a solution-processable approach was applied for fabrication. In brief, the indium−tin oxide (ITO) glass substrate with a sheet resistance of 15 Ω/sq was washed sequentially with a substrate cleaning detergent, dionized water, acetone, and methanol in an ultrasonic bath, followed by UV−ozone treatment prior to use. Then a 30-nm-thick poly(3,4-

ethylenedioxythiophene):poly(styrenesulfonic acid) (PEDOT:PSS; H. C. Starck, Clevios P VP AI 4083) layer was spin-coated onto the ITO and baked in a nitrogen environment at 130 °C for 30 min to remove residual water. Then, 4,4′,4″-tris(carbazol-9-yl)triphenylamine (TCTA) blended with **5** (5 mg + 1 mg + 1 cm^3 of 1,2-dichloroethane) by a spin-coating process (1500 rpm, 60 s) as an emissive layer (EML) was prepared on the PEDOT:PSS layer in order to get a thickness of 50 nm. 1,3,5-Tris(*N*-phenylbenzimidizol-2-yl)benzene (TPBI; 50 nm) as an electron transport layer as well as a hole blocking layer and LiF (0.5 nm) and Al (100 nm) as a typical cathode were evaporated under a vacuum of less than 2×10^{-6} Torr. OLED characterization was performed under a glovebox using a computer-controlled Keithley 6430 source meter and a Keithley 6487 picoammeter equipped with a calibrated silicon photodetector. Electroluminescence (EL) spectra were measured using a photodiode array detector (Ocean Optics USB2000).

Computational Details. The gold(I) clusters **1**−**8** were studied using the hybrid PBE0 density functional.[20] The gold atoms were described by a triple-ζ valence-quality basis set with polarization functions (def2-TZVP).[21] Scalar relativistic effects were taken into account by applying a 60-electron relativistic effective core potential for gold.[22] A split-valence basis set with polarization functions on non-hydrogen atoms was used for all the other atoms.[23] To facilitate comparisons with the experiments, point group symmetry was applied as follows: **1**−**6**, **8**, C_{2h}; **7**, C_{2v} (corresponding to conformer **I** for **1**−**6** and conformer **II** for **7**). The geometries of all complexes were fully optimized. The excited states were investigated with the time-dependent DFT (TD-DFT) approach.[24] The singlet excitations were determined at the optimized ground-state S_0 geometries, while the lowest-energy triplet emissions were determined at the optimized T_1 geometry. All electronic structure calculations were carried out with the *TURBOMOLE* program package (version 6.4).[25]

RESULTS AND DISCUSSION

Synthesis and Structural Characterization. Following the procedure we recently reported,[6] treatment of the neutral triphosphine-based coordination gold complexes P^P^P-$(AuC_2R)_3$ [P^P^P = bis(diphenylphosphinomethyl)-phenylphosphine], in situ generated via depolymerization of the $(AuC_2R)_n$ acetylides, with a stoichiometric amount of trinuclear compound $[Au_3(P^P^P)_2]^{3+}$ results in high-yield formation of the tetranuclear clusters $[Au_4(P^P^P)_2(C_2R)_2]^{2+}$ [R = Ph (**1**), 4-biphenyl (**2**), 4-terphenyl (**3**), 4-OMe-C_6H_4 (**4**), 4-NMe_2-C_6H_4 (**5**), 1-cyclohexanolyl $C_6H_{11}O$ (**6**), 4-$CF_3C_6H_4$ (**7**)], isolated as air- and moisture-stable solids after crystallization (Scheme 1). The same synthetic protocol is valid for the preparation of a thiolate derivative, $[Au_4(P^P^P)_2(SPh)_2]^{2+}$ (**8**).

The crystal structures of the title compounds were determined by the XRD analysis. The structural motif of the tetrametallic clusters **1**−**6** consists of a rhomboidal $\{Au_4\}$ core bridged by two bent P^P^P ligands, which are nearly perpendicular to the plane of the metal framework (see **3**, **5**, and **6** in Figure 2 and ORTEP views of **1**−**6** in Figure S1 in the SI; selected structural parameters are listed in Table 1). Therefore, a general arrangement of complexes **1**−**6** is essentially the same as that found earlier for their chloride congener, $[Au_4(P^P^P)_2Cl_2]^{2+}$,[4e] and the recently reported ferrocenyl-functionalized analogues.[6]

Formation of the metal core is facilitated by aurophilic bonding. The geometry of the metal core is largely determined by ancillary phosphine ligands. A number of tetragold(I) complexes have been reported, with different ligand environments mostly adopting square/rectangular-like[1d,26] or, more rarely, tetrahedral, rhomboidal, or Z-like[1d,27] topologies. The Au−Au distances lie between 3.04034(17) and 3.2325(3) Å,

Scheme 1. Synthesis of Clusters 1−8[a]

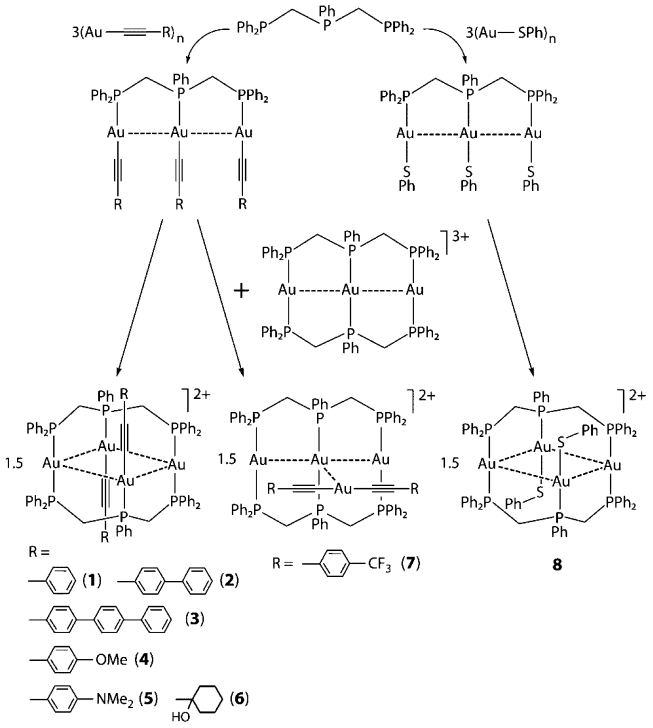

[a]Reaction conditions: CH_2Cl_2, 298 K, 1 h; yield 79−90%; the counterion is PF_6^- except for **6** (ClO_4^-).

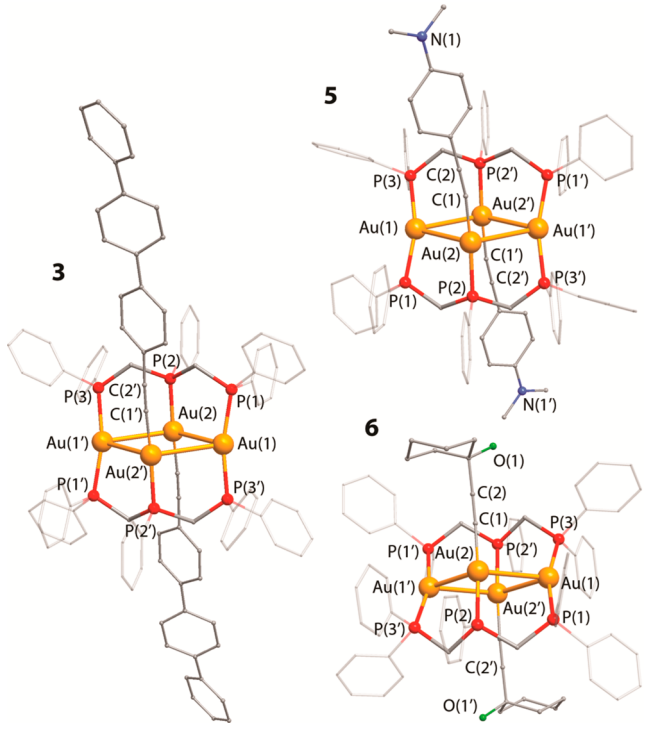

Figure 2. Molecular views of the dications **3**, **5**, and **6**. Symmetry transformations used to generate equivalent atoms (′): in **3**, $1 - x, -y, 1 - z$; in **5**, $1 - x, -y + 1, 1 - z$; in **6**, $-x, -y, 2 - z$.

which is a normal range for effective Au−Au contacts.[1d,28] The values of the P(1)−Au(1)−P(3) and P(2)−Au(2)−C(1) angles (162.92−166.49° and 168.43−170.61°, respectively) visibly deviate from 180° (see Table 1), indicating a distortion

dx.doi.org/10.1021/ic501470v | *Inorg. Chem.* 2014, 53, 12720−12731

Table 1. Selected Bond Lengths and Angles for Complexes 1−6

	1	2	3	4	5	6
			Bond Lengths, Å			
Au(1)−Au(2)	3.07508(14)	3.2325(3)	3.1466(2)	3.11742(12)	3.0810(2)	3.04034(17)
Au(1)−Au(2′)	3.17737(13)	3.0832(3)	3.12815(19)	3.09722(12)	3.0846(2)	3.08838(17)
P(1)−Au(1)	2.3102(6)	2.3137(12)	2.3163(8)	2.3066(5)	2.3070(9)	2.3086(8)
P(2)−Au(2)	2.2863(6)	2.2872(8)	2.2872(8)	2.2903(5)	2.2848(9)	2.2882(8)
C(1)−Au(2)	1.993(3)	1.997(5)	1.995(3)	1.995(2)	2.014(4)	1.995(3)
			Bond Angles, deg			
P(2)−Au(2)−C(1)	169.42(7)	168.43(15)	169.41(9)	169.70(7)	170.61(10)	169.23(10)
P(1)−Au(1)−P(3)	162.92(2)	165.45(5)	166.49(3)	164.27(2)	163.59(3)	163.93(3)

of the linear coordination geometry of Au^I ions probably caused by metal−metal attraction. The structural parameters of **1−6** are very similar to those found for ferrocenyl-containing congeners.[6] The chloro derivative (shown in Figure 1) as well displays very close characteristics of bond lengths and angles within the metal framework.[4e] However, the Au−P distances in $[Au_4(P\text{^}P\text{^}P)_2Cl_2]^{2+}$ are slightly different from those in the alkynyl compound. The central Au(2)−P(2) bond (trans to the chloro ligand) is visibly shorter (2.264 Å) than the analogous value in **1−6** because of the difference in the nature of the trans ligand. On the other hand, the side Au−P contacts in the chloride cluster (2.323 and 2.326 Å) are systematically longer than those in the alkynyl complexes **1−6**. The alkynyl ligands are bound to the corresponding gold centers in η^1-mode; the π systems of the −C≡C− moieties are not involved in bridging of the adjacent metals. This contrasts with other examples of polynuclear gold(I) alkynyl compounds, which are usually formed via σ,π-bridging coordination of the alkyne triple bonds.[1d,2a,l,5a,29] Analysis of the X-ray data did not reveal any systematic correlations between the properties of the alkynyl substituents and the structural parameters of **1−6**.

Surprisingly, the use of alkyne with an electron-accepting group, $-C{\equiv}CC_6H_4CF_3$, leads to the assembly of tetranuclear cluster $[Au_4(P\text{^}P\text{^}P)_2(C_2C_6H_4CF_3)_2]^{2+}$ (**7**), which shows different topology (Scheme 1 and Figures 3 and S2 in the SI). In this complex, the gold atoms form a T-like arrangement that is formally achieved via the addition of the anionic dialkynyl fragment $[Au(C_2C_6H_4CF_3)_2]^-$ to the linear trimetallic motif of the parent compound $[Au_3(P\text{^}P\text{^}P)_2]^{3+}$ to form the unsupported Au(2)−Au(3) bond [3.0092(3) Å].

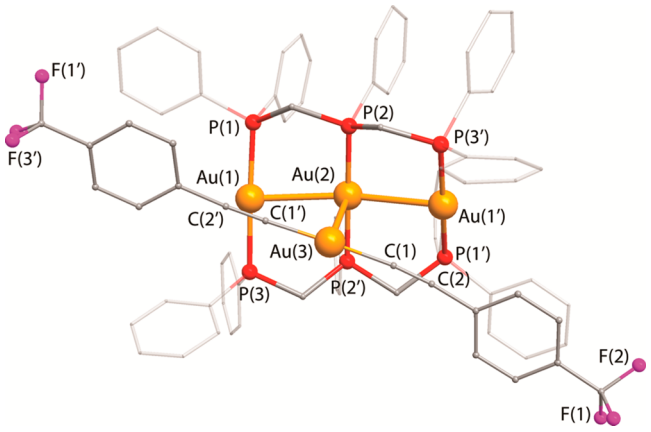

Figure 3. Molecular view of the dication **7**. Selected interatomic distances (Å): C(1)−Au(3) 1.955(7), P(1)−Au(1) 2.3257(9), P(2)−Au(2) 2.3032(9), P(2′)−Au(2) 2.3031(9), P(3)−Au(1) 2.3139(10), Au(1)−Au(2) 2.9855(2), Au(2)−Au(3) 3.0092(3). Symmetry transformations used to generate equivalent atoms (′): 1 − *x*, −*y*, *z*.

The Au(1)−Au(2) distance in the metal core of **7** is slightly longer than the corresponding value in $[Au_3(P\text{^}P\text{^}P)_2]^{3+}$ [2.9855(2) vs 2.9243(2) Å], and the angle Au(1)−Au(2)−Au(1′), 169.9°, is bent in comparison with the linear trigold chain in the parent cluster. The coordination geometry of the $[Au(C_2C_6H_4CF_3)_2]^-$ unit remained virtually unchanged because the C(1)−Au(3)−C(1′) angle (176.2°) is close to 180° and is typical for these kinds of dialkynyl complexes.[30] As in **1−6**, the −C≡C− units of the alkynyl ligands do not participate in binding of the metals because the shortest separation Au(1)−C(1′) exceeds 2.95 Å, which is too long for an appreciable donor−acceptor interaction.

To the best of our knowledge, the T-shape form of a tetragold cluster **7** is unprecedented. A similar structural motif was recently found for the heterometallic Au_2Ag_2 alkynyl complexes.[31] The preference to this structural type might be governed by subtle electronic factors as were found only in the case of the electron-withdrawing alkynyl substituent in the absence of obvious steric hindrances. Unfortunately, we were unable to prepare any complex using an electronically similar ligand, for example, $-C{\equiv}CC_6H_4NO_2$, to confirm the hypothesis.

For the extension or preparative studies, we tested the same synthetic method starting from gold thiolate polymer $(AuSPh)_n$ (Scheme 1) and obtained the tetragold complex **8** in a good yield. The crystal structure of **8** displays a rhomboidal motif analogous to that observed in clusters **1−6** (Figures 4 and S3 in the SI) that points to a particular favorability of the $\{Au_4\}$ framework supported by the P^P^P ligand. The bond lengths and angles in **8** are not exceptional and fit the range of the corresponding values found in **1−6** and in other gold thiolate phosphine compounds.[3g]

NMR Spectroscopic and ESI-MS Characterization. ESI-MS spectra of complexes **1−8** display the dominating signals of doubly charged cations at *m*/*z* 1001.12, 1077.15, 1153.18, 1031.13, 1044.16, 1023.17, 1069.11, and 1009.09, respectively (Figure S4 in the SI). The isotopic patterns observed completely fit the stoichiometry of the corresponding $[Au_4(P\text{^}P\text{^}P)_2(X)_2]^{2+}$ molecular ions, indicating that the composition of the complexes is retained in solution. However, according to the NMR data obtained, the majority of the alkynyl clusters **1−7** exist in a fluid medium as two isomeric species, being in slow chemical equilibria, which depends on the nature of the alkyne and solvent (Scheme 2; see also the ^{31}P NMR data for complex **1** in the Experimental Section).

One of the forms (**I**) is assigned to the structural motif found in the solid state for the rhomboidal complexes **1−6**, whereas the other (**II**) corresponds to the T-shaped molecule stabilized

dx.doi.org/10.1021/ic501470v | Inorg. Chem. 2014, 53, 12720−12731

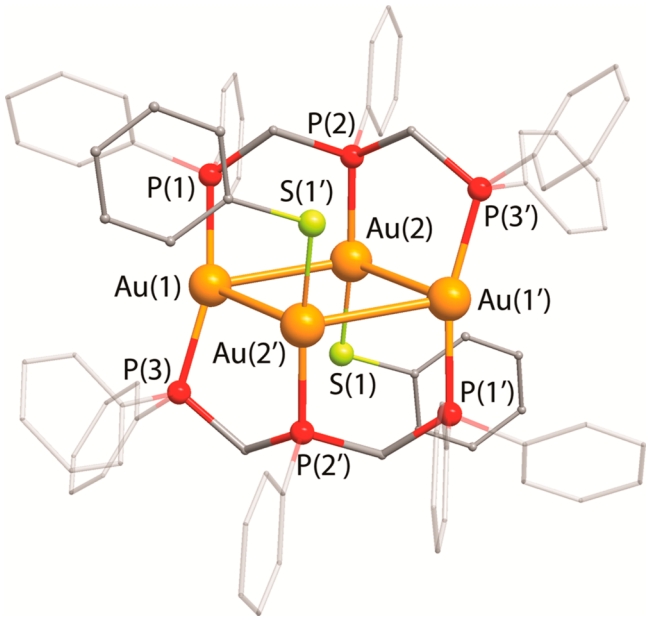

Figure 4. Molecular view of the dication **8**. Selected interatomic distances (Å): S(1)−Au(2) 2.3002(5), Au(1)−Au(2) 3.07057(13), Au(1)−Au(2′) 3.14111(14), P(1)−Au(1) 2.3135(6), P(2)−Au(2) 2.2737(6), P(3)−Au(1) 2.3165(6). Symmetry transformations used to generate equivalent atoms (′): 1 − *x*, 2 − *y*, 1 − *z*.

Scheme 2. Proposed Interconversion of the Isomeric Forms of 1−7[a]

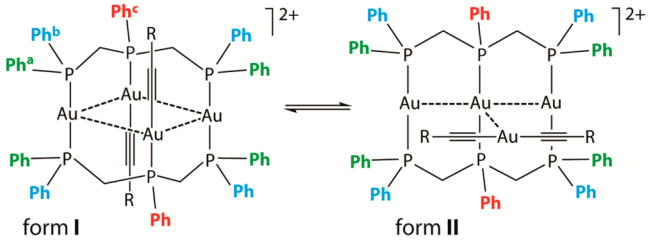

[a]The nonequivalent phenyl rings are indicated according to the assignment of ^{1}H NMR given in the Experimental Section.

in the crystal cell of **7**. Under the conditions described in the Experimental Section and using the freshly prepared solutions, it proved to be possible to minimize the amount of minor species in solution and thus to characterize completely the structure of form **I** using ^{31}P{^{1}H} and ^{1}H NMR spectroscopy. The prolonged standing in solutions that requires equilibrium to be reached results in some degradation of the complexes, which prevents complete assignment of the ^{1}H spectroscopic patterns. In form **I**, which belongs to the C_{2h} symmetry group, the nonequivalent phosphorus nuclei can be organized into two groups (4/2), similar to their close congeners.[6] Two clearly resolved multiplets observed in the ^{31}P{^{1}H} NMR spectra of **1−6** represent an A_4B_2 spin system, with the J_{AB} and J_{AA} coupling networks shown in Figure 5. Simulation of the spin systems in **1−6**, based on the solid-state structural motifs, provides spectroscopic patterns matching the experimental spectra (Figure 5). The values of the coupling constants (J_{AA} ∼ 320 Hz and J_{AB} ∼ 75 Hz) are in good agreement with those found earlier for other transition-metal phosphine complexes.[32]

^{1}H NMR data of rhomboidal form **I** of clusters **1−6** are also compatible with their structural arrangement. The complete

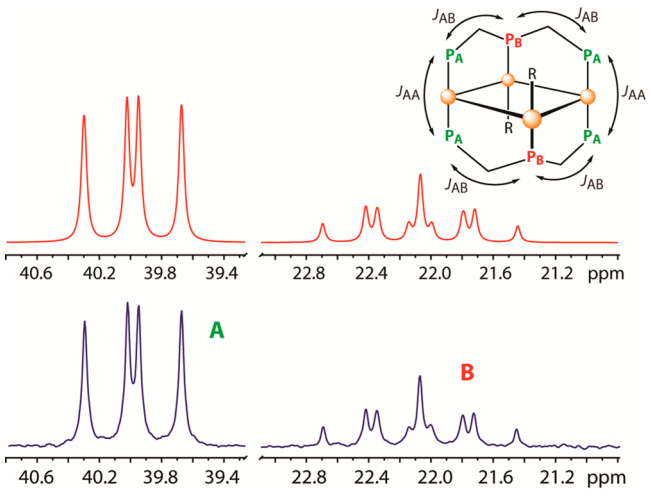

Figure 5. ^{31}P{^{1}H} NMR spectrum of **1**, acetone-d_6, 298 K (bottom). Simulation of the A_4B_2 system: J_{AA} = 320 Hz, J_{AB} = 76 Hz (top). Inset: spin−spin coupling network in form **I**.

assignment of the proton spectra was carried out on the basis of ^{1}H{^{31}P} and ^{1}H−^{1}H COSY measurements (see, e.g., Figure S6 in the SI) and by analogy with recently characterized relatives.[6]

Complex **7**, which shows an isomeric T-shaped structural pattern in the solid state (Figure 3), corresponds to form **II**; see Scheme 2. In solution, **7** displays equilibrium between two isomeric species (see Figure 6), one of which clearly belongs to

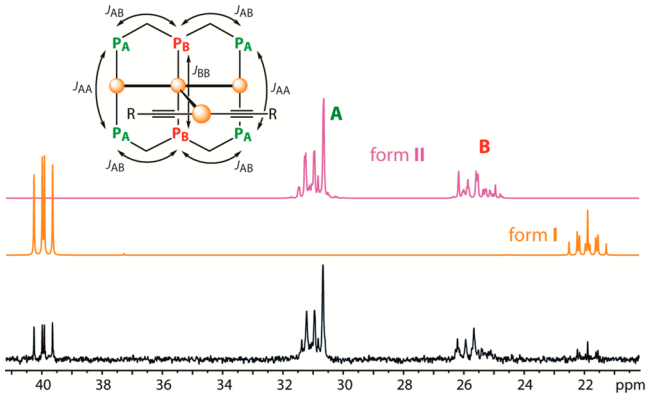

Figure 6. ^{31}P{^{1}H} NMR spectrum of an equilibrated solution of **7**, acetone-d_6, 298 K (bottom). Simulation of A_4B_2 systems: form **I** J_{AA} = 320 Hz, J_{AB} = 75 Hz (top, orange); form **II** J_{AA} = 310 Hz, J_{BB} = 310 Hz, J_{AB} = 74 Hz (top, purple). Inset: spin−spin coupling network in form **II**.

form **I** and displays two typical multiplets at 22 and 40 ppm, observed in the ^{31}P{^{1}H} NMR spectra of the rhomboidal complexes **1−6**. Two other signals in the spectrum may be assigned to the T-shaped form **II** on the basis of the signal simulation, taking into account additional coupling constants in the ^{31}P−^{31}P coupling network. Indeed, the molecule of this type belongs to the idealized C_{2v} symmetry group that generates the A_4B_2 spin system with the coupling scheme shown in the inset of Figure 6.

The simulation made on the basis of this structural/coupling model gave the spectroscopic pattern (Figure 6), where the structure and relative intensities of the signals fit well those observed in the experimental spectrum. Interpretation of the ^{1}H−^{1}H COSY spectrum of **7** (Figure S6 in the SI) also testifies

dx.doi.org/10.1021/ic501470v | *Inorg. Chem.* 2014, 53, 12720−12731

in favor of this structural hypothesis to give three groups (1/2/2) of the phosphine phenyl resonances together with the signals of the $-C_6H_4CF_3$ substituent and methylene spacers. It has to be noted that the relative positions of poorly resolved minor signals in the $^{31}P\{^1H\}$ spectra of **1**–**6** are in good agreement with those found for the major form of **7**, which make it possible to consider the reaction shown in Scheme 2 as a common isomerization equilibrium typical for these types of complexes in solution. The position of the equilibrium is determined by the nature of the alkynyl ligand substituent solvent. It is worth mentioning that the ferrocenyl-functionalized analogues of **1**–**6** do not display appreciable isomerization probably because of the presence of bulky ferrocenyl groups on the alkynyl ligands, which prevent the formation of T-shaped form **II**.[6]

The thiolate complex **8** displays NMR spectroscopic patterns essentially similar to those found for **1**–**6**. The isomeric form **II** was not observed in a solution of **8**, although some minor species of unclear origin were detected upon prolonged standing.

Photophysical Properties. Figures 7 and 8 show absorption and emission spectra of complexes **1**–**8** (see Scheme 1 for the structures) in degassed CH_2Cl_2 and in solid powder, respectively, at room temperature. Note that, for clarity, both Figures 7 and 8 are separated into parts **A** and **B**

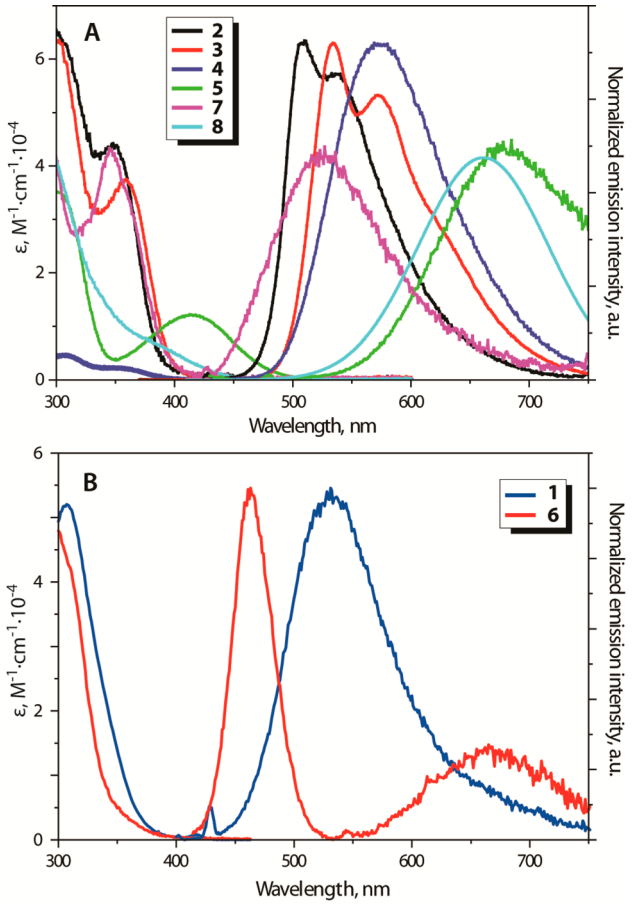

Figure 7. UV–vis absorption (sample concentration = 5×10^{-5} M) and emission spectra of complexes **2**–**5**, **7**, and **8** (A) and **1** and **6** (B) in degassed CH_2Cl_2 (room temperature, λ_{excit} = 360 nm for **1**–**4** and **6**–**8**; λ_{excit} = 420 nm for **5**; the sample absorbance is ~0.1 at the excitation wavelength).

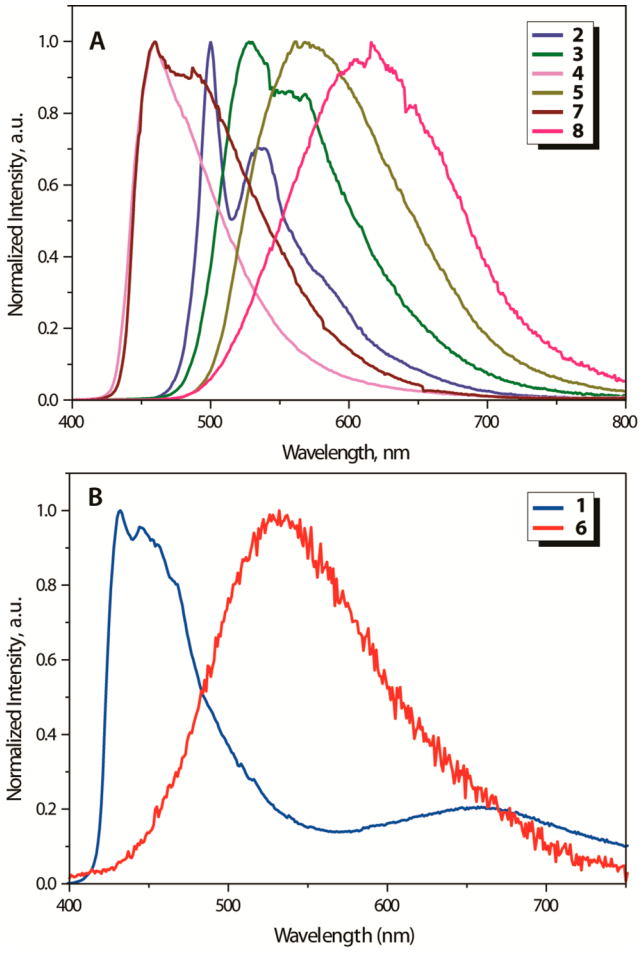

Figure 8. Emission spectra of complexes **2**–**5**, **7**, and **8** (A) and **1** and **6** (B) in the solid state (room temperature, λ_{ex} = 360 nm; the emission is normalized at the peak wavelength).

based on the spectral feature of single- and dual-emission bands (vide infra). For those compounds having similar emission properties in both solution and the solid state, the corresponding spectra are shown in part **A**, while those revealing distinctly different emission features between the aggregation states are ascribed to part **B**. This arrangement also avoids the spectral congestion.

The aforementioned NMR studies have indicated that clusters **1**–**8** undergo isomerization in solution. resulting in two isomeric species being in slow chemical equilibria. Therefore, it is reasonable to propose the observed emission in solution originating from isomer **I** or **II** or the equilibrium between **I** and **II** to account for the dual emission. The single-emission bands for compounds **2**–**5**, **7**, and **8** in degassed CH_2Cl_2 are evidenced not only by the steady-state phosphorescence (Figure 7A) but also by the single-exponential emission decay kinetics (see Table 2) and the same excitation spectra monitored throughout the emission band. The vibronic progressions were determined for clusters **2** and **3** ($\Delta\nu$ = 1063 and 1248 cm^{-1}, respectively), which probably originate from the phenylene fragments of the alkynyl ligands. Moreover, the spectral features for **2**–**5**, **7**, and **8** are also similar to their corresponding emission spectra in the solid state (Figure 8A). On the basis of their single-crystal X-ray structure, the results clearly indicate that the emission of complexes **2**–**5** and **8** mainly originates from the conformer **I**, while that of complex **7**

dx.doi.org/10.1021/ic501470v | Inorg. Chem. 2014, 53, 12720–12731

Table 2. Photophysical Properties of Complexes 1−8 and of the Starting $[Au_3(P\text{^}P\text{^}P)_2](PF_6)_3$ at Room Temperature

	λ_{ab}/nm	ε (10^{-4})	$\lambda_{em}{}^a$/nm	$\lambda_{em}{}^b$/nm	Φ^a	Φ^b	$\tau_{obs}{}^a/\mu s$	χ^2	$\tau_{obs}{}^b/\mu s$	χ^2	$\tau_r{}^c/\mu s$
Au_3	344	7.71	460, 665	460	0.09	0.90	1.62 (460 nm), 4.01 (665 nm)	1.07, 1.00	2.14	1.32	18.00, 44.60
$Au_4Cl_2{}^d$	ca. 295	ca. 4.2	ca. 515								
1	308	5.09	533	440, 650	0.01	0.26	0.29 (530 nm)	1.11	7.54 (440 nm), 11.74 (650 nm)	1.12, 1.28	59.16
2	350	4.37	510	520	0.05	0.15	6.97	1.21	18.10	1.04	137.93
3	361	4.22	550	543	0.25	0.09	3.20	1.12	16.30	1.12	13.04
4	354	0.25	577	460	0.07	0.44	1.80	1.16	7.59	1.45	27.53
5	414	1.38	676	573	0.01	0.51	0.01	0.72	1.94	0.97	1
6	300	4.79	460, 670	530	0.03	0.30	2.97 (460 nm), 8.17 (670 nm)	1.19, 1.15	4.51	1.11	99.00 (460 nm), 272.33 (670 nm)
7	348	4.80	528	477	0.02	0.22	0.37	1.06	5.06	1.51	14.96
8	393	0.67	666	615	0.01	0.07	0.11	0.93	0.88	1.39	11

[a]Measured in degassed CH_2Cl_2. [b]Measured in the solid state. [c]τ_r is deduced from data obtained in the degassed solution, $\tau_r = \tau_{obs}/\Phi$. [d]Complex $[Au_4(P\text{^}P\text{^}P)_2Cl_2][CF_3SO_3]$.[4e] For the solution quantum yield (Φ) measurements, coumarin 480 in methanol ($\Phi_{em} \sim 0.87$) is used as the standard. λ_{ex} = 380 nm; sample concentrations in the range 10^{-5}−10^{-6} M were used to determine the absorption extinction coefficients and quantum yield measurements.

is from conformer **II**. Complex **1** demonstrated limited photostability under steady-state irradiation, which leads to the appearance of some uncharacterized species due to photodegradation.

As depicted in Figures 7B and 8B, the emission profile for **1** in the solid state is much different from that in degassed CH_2Cl_2. In a deaerated solution, the emission of **1** fits well to the category of complexes in Figure 7A, showing a single-emission band maximized at 533 nm. In sharp contrast, in spite of the fact that only one type of species was characterized for **1** in the solid state using single-crystal X-ray analysis (vide supra), dual emission was observed in the solid state maximized at 440 and 650 nm. Further temperature-dependent studies of complex **1** in the solid state show nearly temperature independence (Figure S7 in the SI). Therefore, the dual emission of complex **1** very probably arises from the crystalline inhomogeneity of a bulk sample due to the fast loss of the crystallization solvent, which is accompanied by visible changes of the photoluminescent properties (Figure S8 in the SI). The changes in packing may lead to the presence of at least two crystalline phases, which can have contrasting emission properties, as we have recently shown for the hexanuclear gold complexes.[5b]

Complex **6** shows regular emission in the solid state, i.e., a single-emission band maximum at 530 nm that originates from conformer **I**. However, among the title complexes, **6** apparently is the only one that exhibits dual emission in a CH_2Cl_2 solution. Monitoring the emission maxima of 460 and 670 nm, we found that the peak wavelengths of the corresponding excitation spectrum appear at 350 and 362 nm, respectively (Figure S9 in the SI). Also, the 460 and 670 nm bands give distinctly different emission lifetimes of 2.97 and 8.17 μs. These results clearly indicate the existence of two different ground-state species for complex **6**, in which the 460 nm emission band, similar to other congeners, originates from conformer **I**. To further identify the origin of the 670 nm emission band, we then carefully performed a concentration-dependent study and found that the intensity ratio for the dual emission was independent of the concentration in the range of 10^{-6}−10^{-4} M. The results discard a proposal that the dual emission could possibly be derived from colligative phenomena such as a dimer or an excimer. Alternatively, we tentatively assign the 670 nm band to some other isomeric species (e.g., conformer **II** emission). A lack of conformer **II** emission for the rest of the title complexes can be attributed to vibrational quenching or to their small content in the system. Note that the emission gap of conformer **I** for complex **6** is the largest among the studied clusters (see Figure 7) perhaps because of the nonaromatic terminal substituent R (see Scheme 1). Accordingly, the associated conformer **II** emission (670 nm) for **6** is to be in the highest energy among all title complexes. It is thus reasonable to expect that the conformer **II** emission of **1**−**5**, if it exists, might be in the range of ≫700 nm. Governed by the energy gap law[33] operative for the organic and organometallic compounds, such a low-band-gap near-IR emission, in theory, is subject to dramatic vibrational quenching, giving virtually no emission.

The quantum yield of the crystalline trigold complex $[Au_3(P\text{^}P\text{^}P)_2](PF_6)_3$ was determined to be 0.9, which is visibly higher than the value (0.64) reported recently for the same compound in the KBr tablet form.[9] This difference may be attributed to the changes of the crystal lattice induced by grinding during the tablet preparation.

Computational Studies. We investigated the photophysical properties of the gold(I) clusters **1**−**8** using quantum chemical methods. The geometries of the studied complexes were optimized at the DFT−PBE0 level of theory, after which the lowest-energy singlet and triplet excited states were characterized with TD-DFT−PBE0 calculations (see the Experimental Section for full computational details). Structural optimizations, carried out in the gas phase, reproduce the experimentally observed structures reasonably well. The differences in the key Au−Au distances between the X-ray and computational structures vary from 0.03 Å (**7**) to 0.23 Å (**6**).

The wavelengths predicted for the $S_0 \rightarrow S_1$ and $T_1 \rightarrow S_0$ electronic transitions are listed in Table 3, and the corresponding electron density difference plots are visualized in Figure 9 for clusters **1**, **7**, and **8** (clusters **2**−**6** are illustrated in the SI). For clusters **1**−**5**, the studied transitions are rather similar in nature and can be described as combinations of alkynyl intraligand $\pi \rightarrow \pi^*$ transitions and Au-to-alkyne metal-to-ligand charge transfer. The transitions do not involve any significant contributions from the phosphine ligands. The predicted $S_0 \rightarrow S_1$ absorption wavelengths are somewhat red-

dx.doi.org/10.1021/ic501470v | Inorg. Chem. 2014, 53, 12720−12731

Table 3. Computational Photophysical Results for Gold(I) Clusters 1−8 (PBE0−TD-DFT)

	λ_{ab}, $S_0 \rightarrow S_1$ (nm)		λ_{em}, $T_1 \rightarrow S_0$ (nm)	
	theor[a]	exp	theor	exp[b]
1	336 (0.30)	308	488	443
2	397 (0.59)	350	581	520
3	465 (0.63)	361	638	543
4	382 (0.29)	354	500	460
5	461 (0.27)	414	560	573
6	291 (0.02)	300	372	459
7	360 (0.30)	348	517	477
8	348 (0.14)	393	537	615

[a]Oscillator strengths are given in parentheses. [b]Emission wavelengths are measured in the solid state.

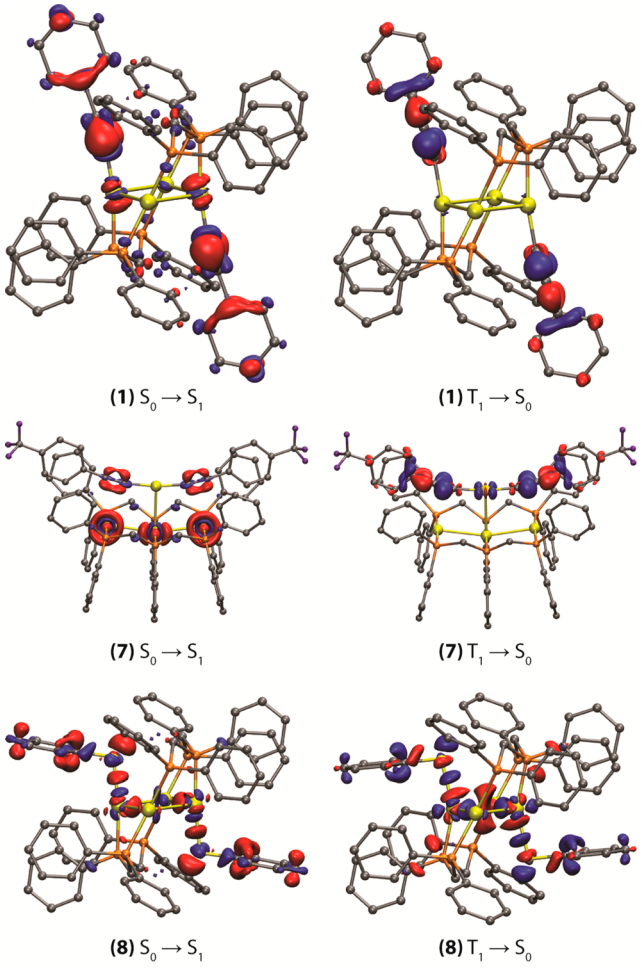

Figure 9. Electron density difference plots for the lowest-energy singlet excitation ($S_0 \rightarrow S_1$) and the lowest-energy triplet emission ($T_1 \rightarrow S_0$) of gold(I) clusters **1**, **7**, and **8** (isovalue 0.002 au). During the electronic transition, the electron density increases in the blue areas and decreases in the red areas. Hydrogen atoms are omitted for clarity.

shifted in comparison to the experiment, except for **6** and **8**, where the predicted wavelengths are blue-shifted instead. The TD-DFT calculations reproduce the experimentally observed trend, where the absorption wavelength increases as the length of the alkynyl ligand increases for **1**−**3**. The same increasing trend within clusters **1**−**3** is reproduced also for the $T_1 \rightarrow S_0$ emission wavelengths. The structural relaxation arising from the geometry optimization of the T_1 state is rather small: e.g., for clusters **1**−**5**, the Au−Au contacts shorten by ca. 0.05 Å. A comparison of the electron density differences reveals that the contribution of the gold atoms to the excited states decreases in the order **1** > **2** > **3**. For **4** and **5**, the contribution of the gold atoms is again larger in comparison to **3**. For cluster **6** with R = $C_6H_{11}O$, the $T_1 \rightarrow S_0$ transition predicted by TD-DFT is centered on the phosphine ligand and probably does not correspond to the experimentally observed transition. However, we were unable to locate a T_1 geometry showing a longer emission wavelength. The excited-state characteristics of clusters **7** and **8** are different from those of **1**−**5**, as can be expected from their different structural characteristics. In both cases, the gold atoms show a major contribution to the excited states.

Device Fabrication and Properties. Figure 10 depicts the UV−vis absorption and PL spectra of cluster **5** recorded from a

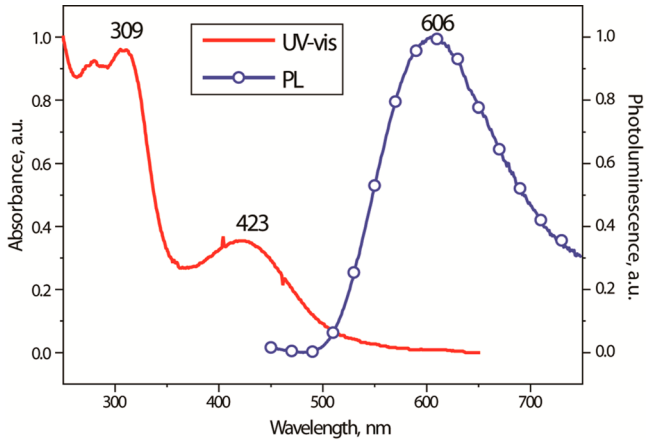

Figure 10. UV−vis absorption and emission spectra of cluster **5** in a neat film.

neat film on a quartz substrate. The UV−vis spectrum exhibits two absorption maxima (λ_{max}) centered at 309 and 423 nm. In solution, **5** shows a broad emission band at ∼580 nm upon excitation at 350 nm (Figure 9). A characteristic red shift of ca. 26 nm of the PL spectrum in the film state (λ_{max} = 606 nm) is thought to be related to the formation of intermolecular aggregation. In addition, an excellent PL quantum yield of cluster **5** is 0.51, which is anticipated to exhibit a promising potential as a candidate of emitting material for the fabrication of high-performance OLEDs.

To investigate the charge-carrier injection properties of **5**, we estimated the energy level of the HOMO to be −5.47 eV by atmospheric photoelectron spectroscopy. Through subtraction of the optical energy gap (E_g = 2.42 eV) from the HOMO energy level, we calculated the energy level of the LUMO to be −3.05 eV.

To evaluate the EL properties of the gold(I) cluster complexes, solution-processed OLEDs were fabricated using TCTA as the host, with **5** as the dopant for an EML in the structure: ITO/PEDOT:PSS (30 nm)/EML (50 nm)/TPBI (50 nm)/LiF (0.5 nm)/Al (100 nm). To improve the hole injection from the anode, PEDOT:PSS was spun onto the precleaned ITO substrate to form a polymer buffer layer. TCTA is a well-known hole-transporting material with a good hole mobility of 3.0×10^{-4} $cm^2/V{\cdot}s$ and suitable HOMO/LUMO levels of −5.7/−2.4 eV.[34] The energy level diagram

dx.doi.org/10.1021/ic501470v | Inorg. Chem. 2014, 53, 12720−12731

shows that the HOMO and LUMO energy levels of **5** (−5.47/−3.05 eV) lie above and below those of the TCTA host, respectively, to confine both electrons and holes within an EML. To further confine the holes or generated excitons within the emissive region, TPBI[35] was thermally evaporated onto the spin-coated EML as an electron-transport layer as well as a hole-blocking layer because of the high-lying HOMO level. LiF and Al served as the electron-injecting layer and cathode, respectively.

Figure 11 depicts the current density−voltage−luminance (J−V−L) characteristics, device efficiency, and EL spectrum of the device. The device displayed a low turn-on voltage of 2.5 V and a maximum brightness (L_{max}) as high as 7430 cd/m^2 at 10 V (980 mA/cm^2), achieving a maximum external quantum efficiency (η_{ext}) of 3.1% corresponding to a current efficiency (η_c) of 6.1 cd/A and a power efficiency (η_p) of 5.3 lm/W. The EL spectrum shows a broad band with a maximum at ∼600 nm, a full width at half maxima (fwhm) of 126 nm, and Commission Internationale de l'Eclairage (CIE) coordinates of (0.52, 0.46), resembling that of the PL spectrum in the solid thin film. A very few gold(I) complexes, e.g., [Au(4-R-dppn)$_2$]X [dppn = 1,8-bis(diphenylphosphino)naphthalene; R = H, Me] or [Au$_2$(dppm)$_2$]$^{2+}$ [dppm = bis(dipehenylphosphino)methane], were employed earlier as triplet emitters in EL devices.[36] However, only very low quantum efficiencies were obtained (<0.1−0.02%), which are orders of magnitude lower the value that we reached in the current work. The overall result showed that, although the device performance has not been fully optimized yet, the combination of high efficiency and solution processability of OLEDs that employ polynuclear gold(I) cluster complexes makes them promising candidates for use as dopant emitters in light-emitting diode devices.

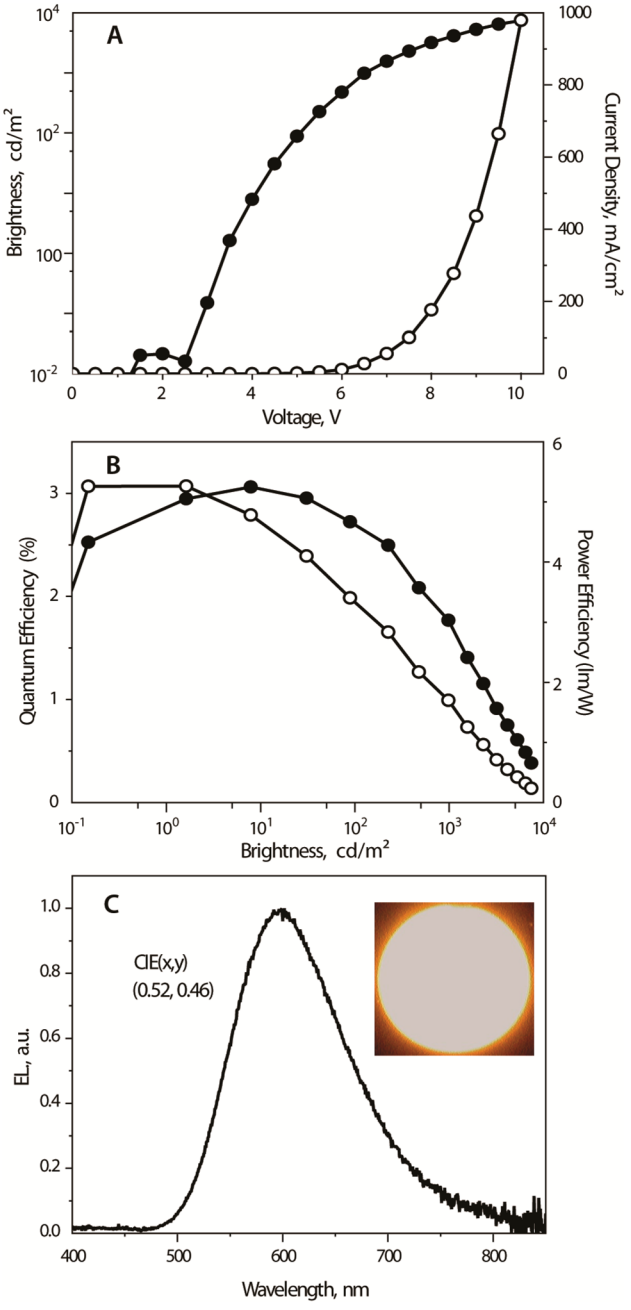

Figure 11. (A) Brightness (●) and current density (○) versus voltage characteristics, (B) external quantum (●) and power (○) efficiencies as a function of the brightness, and (C) a normalized EL spectrum of the device with **5** as the dopant.

CONCLUSION

We have described the preparation of a series of tetragold(I) clusters supported by the triphosphine ligand $PPh_2CH_2PPhCH_2PPh_2$ (P^P^P). Depolymerization of $(AuXR)_n$ (X = C_2, S) with P^P^P and subsequent coupling of intermediate complex (P^P^P)$(AuXR)_3$ with cationic species $[Au_3(P^P^P)_2]^{3+}$ lead to a clean formation of novel compounds of the general formula $[Au_4(P^P^P)_2(XR)_2]^{2+}$ (**1**−**8**). According to the XRD data, these clusters adopt two structural motifs in the solid state: complexes of form **I** with a rhomboidal Au_4 core [X = C_2; R = Ph (**1**), biphenyl (**2**), terphenyl (**3**), C_6H_4OMe (**4**), $C_6H_4NMe_2$ (**5**), $C_6H_{11}O$ (**6**); X = S; R = Ph (**8**)] and complex **7** (X = C_2; R = $C_6H_4CF_3$), which shows a T-shaped arrangement of metal ions (form **II**).

The NMR and ESI-MS spectroscopic studies revealed that these compounds retain their composition in solution but in a fluid medium exist as two isomeric species (forms **1** and **II**), being in slow chemical equilibria, which depend on the solvent and chemical nature of the constituting ligands.

All of these complexes are photoluminescent both in the solid state and in solution. However, because of the low intensity of emission in solution and the presence of two isomeric forms, the focus has been on the photophysical investigations in the solid state, where the title clusters exhibit moderate-to-strong phosphorescence having maxima in a wide range of energies from 443 to 615 nm, reaching a quantum yield of 0.51 (**5**). DFT calculations support the experimental studies and demonstrate the important role of gold atoms with variable contribution of the alkyne ligands in the excitation and emission properties of complexes **1**−**8**.

A relatively high quantum efficiency of cluster **5** allowed for employment of this luminophore in the fabrication of an OLED device that has been achieved for the first time among polynuclear gold(I) compounds. A decent device performance is reported with an external quantum efficiency of 3.1%, corresponding to a current efficiency of 6.1 cd/A and a power efficiency of 5.3 lm/W, with CIE coordinates of (0.52, 0.46).

ASSOCIATED CONTENT

Supporting Information

X-ray crystallographic data in CIF for **1**−**8**, ESI-MS and additional NMR spectroscopic data, additional figures, and

dx.doi.org/10.1021/ic501470v | Inorg. Chem. 2014, 53, 12720−12731

optimized Cartesian coordinates of the studied systems. This material is available free of charge via the Internet at http://pubs.acs.org.

AUTHOR INFORMATION

Corresponding Authors

*E-mail: stunik@inbox.ru.
*E-mail: chop@ntu.edu.tw.
*E-mail: igor.koshevoy@uef.fi.

Notes

The authors declare no competing financial interest.

ACKNOWLEDGMENTS

The authors appreciate the financial support received from the University of Eastern Finland (strategic funding: Russian−Finnish collaborative project and Spearhead projects), Academy of Finland (Grant 268993/2013 to I.O.K.), Alfred Kordelin Foundation (to A.J.K.), St. Petersburg State University (Research Grant 0.37.169.2014), and Russian Foundation for Basic Research (Grant 14-03-00970-a). Computational resources were provided by CSC, the Finnish IT Center for Science (to A.J.K.). NMR studies were performed at the Centers for Magnetic Resonance of St. Petersburg State University.

REFERENCES

(1) (a) Pyykko, P. *Angew. Chem., Int. Ed.* **2004**, *43*, 4412−4456. (b) Crespo, O. Gold−Gold Interactions. In *Modern Supramolecular Gold Chemistry*; Laguna, A., Ed.; Wiley-VCH: Weinheim, Germany, 2008; pp 65−131. (c) Schmidbaur, H.; Schier, A. *Chem. Soc. Rev.* **2008**, *37*, 1931−1951. (d) Schmidbaur, H.; Schier, A. *Chem. Soc. Rev.* **2012**, *41*, 370−412.

(2) (a) Mingos, D. M. P.; Yau, J.; Menzer, S.; Williams, D. J. *Angew. Chem., Int. Ed.* **1995**, *34*, 1894−1895. (b) Lee, Y.-A.; Eisenberg, R. *J. Am. Chem. Soc.* **2003**, *125*, 7778−7779. (c) Chen, J.; Mohamed, A. A.; Abdou, H. E.; Bauer, J. A. K.; Fackler, J. P. J.; Bruce, A. E.; Bruce, M. R. M. *Chem. Commun.* **2005**, *1575−1577*. (d) Yu, S.-Y.; Zhang, Z.-X.; Cheng, E. C.-C.; Li, Y.-Z.; Yam, V. W.-W.; Huang, H.-P.; Zhang, R. *J. Am. Chem. Soc.* **2005**, *127*, 17994−17995. (e) Chui, S. S.-Y.; Chen, R.; Che, C.-M. *Angew. Chem., Int. Ed.* **2006**, *45*, 1621−1624. (f) Yu, S.-Y.; Sun, Q.-F.; Lee, T. K.-M.; Cheng, E. C.-C.; Li, Y.-Z.; Yam, V. W.-W. *Angew. Chem., Int. Ed.* **2008**, *47*, 4551−4554. (g) Sun, Q.-F.; Kwok-Ming Lee, T.; Li, P.-Z.; Yao, L.-Y.; Huang, J.-J.; Huang, J.; Yu, S.-Y.; Li, Y.-Z.; Cheng, E. C.-C.; Yam, V. W.-W. *Chem. Commun.* **2008**, 5514−5516. (h) Puddephatt, R. J. *Chem. Soc. Rev.* **2008**, *37*, 2012−2027. (i) Abdou, H. E.; Mohamed, A. A.; Fackler, J. P. J. Gold(I) Nitrogen Chemistry. In *Gold Chemistry*; Mohr, F., Ed.; Wiley-VCH: Weinheim, Germany, 2009; pp 1−46. (j) Gimeno, M. C.; Laguna, A. *Chem. Soc. Rev.* **2008**, *37*, 1952−1966. (k) Lee, T. K.-M.; Zhu, N.; Yam, V. W.-W. *J. Am. Chem. Soc.* **2010**, *132*, 17646−17648. (l) Koshevoy, I. O.; Lin, C.-L.; Karttunen, A. J.; Haukka, M.; Shih, C.-W.; Chou, P.-T.; Tunik, S. P.; Pakkanen, T. A. *Chem. Commun.* **2011**, *47*, 5533−5535. (m) Lima, J. C.; Rodriguez, L. *Chem. Soc. Rev.* **2011**, *40*, 5442−5456.

(3) (a) Forward, J. M.; Bohmann, D.; Fackler, J. P. J.; Staples, R. J. *Inorg. Chem.* **1995**, *34*, 6330−6336. (b) Lagunas, M. C.; Fierro, C. M.; Pintado-Alba, A.; de la Riva, H.; Betanzos-Lara, S. *Gold Bull.* **2007**, *40*, 135−141. (c) Yam, V. W.-W.; Cheng, E. C.-C. *Top. Curr. Chem.* **2007**, *281*, 269−309. (d) Yam, V. W.-W.; Cheng, E. C.-C. *Chem. Soc. Rev.* **2008**, *37*, 1806−1813. (e) Che, C.-M.; Lai, S.-W. Luminescence and Photophysics of Gold Complexes. In *Gold Chemistry*; Mohr, F., Ed.; Wiley-VCH: Weinheim, Germany, 2009; pp 249−282. (f) López-de-Luzuriaga, J. M. Luminescence of Supramolecular Gold-Containing Materials. In *Modern Supramolecular Gold Chemistry*; Laguna, A., Ed.; Wiley-VCH: Weinheim, Germany, 2008; pp 347−402. (g) Tiekink, E. R. T.; Kang, J.-G. *Coord. Chem. Rev.* **2009**, *253*, 1627−1648. (h) Lotito, K. J.; Peters, J. C. *Chem. Commun.* **2010**, *46*, 3690−3692. (i) He, X.; Yam, V. W.-W. *Coord. Chem. Rev.* **2011**, *255*, 2111−2123.

(4) (a) King, C.; Wang, J. C.; Khan, M. N. I.; Fackler, J. P. J. *Inorg. Chem.* **1989**, *28*, 2145−2149. (b) Li, D.; Che, C.-M.; Peng, S.-M.; Liu, S.-T.; Zhou, Z.-Y.; Mak, T. C. W. *J. Chem. Soc., Dalton Trans.* **1993**, 189−194. (c) Yam, V. W.-W.; Choi, S. W.-K. *J. Chem. Soc., Dalton Trans.* **1994**, 2057−2059. (d) Xiao, H.; Weng, Y.-X.; Wong, W.-T.; Mak, T. C. W.; Che, C.-M. *J. Chem. Soc., Dalton Trans.* **1997**, 221−226. (e) Bardaji, M.; Laguna, A.; Orera, V. M.; Villacampa, M. D. *Inorg. Chem.* **1998**, *37*, 5125−5130. (f) Zank, J.; Schier, A.; Schmidbaur, H. *J. Chem. Soc., Dalton Trans.* **1998**, 323−324. (g) Tanase, T.; Masuda, K.; Matsuo, J.; Hamaguchi, M.; Begum, R. A.; Yano, S. *Inorg. Chim. Acta* **2000**, *299*, 91−99. (h) Bardaji, M.; Laguna, A. *Inorg. Chim. Acta* **2001**, *318*, 38−44. (i) Sevillano, P.; Langetepe, T.; Fenske, D. *Z. Anorg. Allg. Chem.* **2003**, *629*, 207−214. (j) Yip, S.-K.; Lam, W. H.; Zhu, N.; Yam, V. W.-W. *Inorg. Chim. Acta* **2006**, *359*, 3639−3648. (k) Gimeno, M. C. The Chemistry of Gold. In *Modern Supramolecular Gold Chemistry*; Laguna, A., Ed.; Wiley-VCH: Weinheim, Germany, 2008; pp 1−64. (l) Tong, G. S. M.; Kui, S. C. F.; Chao, H.-Y.; Zhu, N.; Che, C.-M. *Chem.—Eur. J.* **2009**, *15*, 10777−10789. (m) Takemura, Y.; Takenaka, H.; Nakajima, T.; Tanase, T. *Angew. Chem., Int. Ed.* **2009**, *48*, 2157−2161.

(5) (a) Koshevoy, I. O.; Chang, Y.-C.; Karttunen, A. J.; Selivanov, S. I.; Jänis, J.; Haukka, M.; Pakkanen, T. A.; Tunik, S. P.; Chou, P.-T. *Inorg. Chem.* **2012**, *51*, 7392−7403. (b) Koshevoy, I. O.; Chang, Y.-C.; Chen, Y.-A.; Karttunen, A. J.; Grachova, E. V.; Tunik, S. P.; Jänis, J.; Pakkanen, T. A.; Chou, P.-T. *Organometallics* **2014**, *33*, 2363−2371.

(6) Dau, T. M.; Shakirova, J. R.; Doménech, A.; Jänis, J.; Haukka, M.; Grachova, E. V.; Pakkanen, T. A.; Tunik, S. P.; Koshevoy, I. O. *Eur. J. Inorg. Chem.* **2013**, 4976−4983.

(7) Appel, R.; Geisler, K.; Schöler, H.-F. *Chem. Ber.* **1979**, *112*, 648−653.

(8) Shakirova, J. R.; Grachova, E. V.; Melekhova, A. A.; Krupenya, D. V.; Gurzhiy, V. V.; Karttunen, A. J.; Koshevoy, I. O.; Melnikov, A. S.; Tunik, S. P. *Eur. J. Inorg. Chem.* **2012**, 4048−4056.

(9) Dau, T. M.; Shakirova, J. R.; Karttunen, A. J.; Grachova, E. V.; Tunik, S. P.; Melnikov, A. S.; Pakkanen, T. A.; Koshevoy, I. O. *Inorg. Chem.* **2014**, *53*, 4705−4715.

(10) Coates, G. E.; Parkin, C. *J. Chem. Soc.* **1962**, 3220−3226.

(11) Raisanen, M. T.; Runeberg, N.; Klinga, M.; Nieger, M.; Bolte, M.; Pyykko, P.; Leskela, M.; Repo, T. *Inorg. Chem.* **2007**, *46*, 9954−9960.

(12) *APEX2—Software Suite for Crystallographic Programs*; Bruker AXS, Inc.: Madison, WI, 2009.

(13) Sheldrick, G. M. *Acta Crystallogr., Sect. A* **2008**, *A64*, 112−122.

(14) Farrugia, L. J. *J. Appl. Crystallogr.* **1999**, *32*, 837−838.

(15) Sheldrick, G. M. *SADABS-2008/1—Bruker AXS area detector scaling and absorption correction*; Bruker AXS: Madison, WI, 2008.

(16) Spek, A. L. *PLATON, A Multipurpose Crystallographic Tool*; Utrecht University: Utrecht, The Netherlands, 2005.

(17) Huang, P.-H.; Shen, J.-Y.; Pu, S.-C.; Wen, Y.-S.; Lin, J. T.; Chou, P.-T.; Yeh, M.-C. P. *J. Mater. Chem.* **2006**, *16*, 850−857.

(18) Demas, J. N.; Crosby, G. A. *J. Phys. Chem.* **1971**, *75*, 991−1024.

(19) de Mello, J. C.; Wittmann, H. F.; Friend, R. H. *Adv. Mater.* **1997**, *9*, 230−232.

(20) (a) Perdew, J. P.; Burke, K.; Ernzerhof, M. *Phys. Rev. Lett.* **1996**, *77*, 3865−3868. (b) Adamo, C.; Barone, V. *J. Chem. Phys.* **1999**, *110*, 6158−6170.

(21) Weigend, F.; Ahlrichs, R. *Phys. Chem. Chem. Phys.* **2005**, *7*, 3297−3305.

(22) Andrae, D.; Häußermann, U.; Dolg, M.; Stoll, H.; Preuß, H. *Theor. Chem. Acc.* **1990**, *77*, 123−141.

(23) Schäfer, A.; Horn, H.; Ahlrichs, R. *J. Chem. Phys.* **1992**, *97*, 2571−2577.

(24) (a) Furche, F.; Rappoport, D. Density Functional Methods for Excited States: Equilibrium Structure and Electronic Spectra. In *Computational Photochemistry*; Olivucci, M., Ed.; Elsevier: Amsterdam, The Netherlands, 2005; pp 93−128. (b) Furche, F.; Ahlrichs, R. *J. Chem. Phys.* **2002**, *117*, 7433−7447. (c) van Wüllen, C. *J. Comput. Chem.* **2011**, *32*, 1195−1201.

(25) Ahlrichs, R.; Bär, M.; Häser, M.; Horn, H.; Kölmel, C. *Chem. Phys. Lett.* **1989**, *162*, 165−169.
(26) (a) Wang, S.; Fackler, J. P. J. *Inorg. Chem.* **1990**, *29*, 4404−4407. (b) Schmidbaur, H.; Gabbai, F. P.; Schier, A.; Riede, J. *Organometallics* **1995**, *14*, 4969−4971. (c) López-de-Luzuriaga, J. M.; Sladek, A.; Schneider, W.; Schmidbaur, H. *Chem. Ber.* **1997**, *130*, 641−646. (d) Chen, J.; Jiang, T.; Wei, G.; Mohamed, A. A.; Homrighausen, C.; Bauer, J. A. K.; Bruce, A. E.; Bruce, M. R. M. *J. Am. Chem. Soc.* **1999**, *121*, 9225−9226. (e) Koshevoy, I. O.; Haukka, M.; Selivanov, S. I.; Tunik, S. P.; Pakkanen, T. A. *Chem. Commun.* **2010**, *46*, 8926−8928.
(27) (a) Zeller, E.; Beruda, H.; Kolb, A.; Bissinger, P.; Riede, J.; Schmidbaur, H. *Nature* **1991**, *352*, 141−3. (b) Ehlich, H.; Schier, A.; Schmidbaur, H. *Organometallics* **2002**, *21*, 2400−2406. (c) Himmelspach, A.; Finze, M.; Raub, S. *Angew. Chem., Int. Ed.* **2011**, *50*, 2628−2631.
(28) Pyykkö, P. *Chem. Soc. Rev.* **2008**, *37*, 1967−1997.
(29) (a) Yip, S.-K.; Cheng, E. C.-C.; Yuan, L.-H.; Zhu, N.; Yam, V. W.-W. *Angew. Chem., Int. Ed.* **2004**, *43*, 4954−4957. (b) Blanco, M. C.; Camara, J.; Gimeno, M. C.; Jones, P. G.; Laguna, A.; Lopez-de-Luzuriaga, J. M.; Olmos, M. E.; Villacampa, M. D. *Organometallics* **2012**, *31*, 2597−2605.
(30) Manbeck, G. F.; Brennessel, W. W.; Stockland, J.; Robert, A.; Eisenberg, R. *J. Am. Chem. Soc.* **2010**, *132*, 12307−12318.
(31) Xu, L.-J.; Wang, J.-Y.; Zhang, L.-Y.; Shi, L.-X.; Chen, Z.-N. *Organometallics* **2013**, *32*, 5402−5408.
(32) (a) Tunik, S. P.; Vlasov, A. V.; Kogdov, K. V.; Starova, G. L.; Nikol'skii, A. B.; Manole, O. S.; Struchkov, Y. T. *J. Organomet. Chem.* **1994**, *479*, 59−72. (b) Koshevoy, I. O.; Tunik, S. P.; Jaaskelainen, S.; Haukka, M.; Pakkanen, T. A.; Podkorytov, I. S. *J. Chem. Soc., Dalton Trans.* **2002**, 2768−2774.
(33) Caspar, J. V.; Meyer, T. J. *J. Phys. Chem.* **1983**, *87*, 952−957.
(34) (a) Su, S.-J.; Gonmori, E.; Sasabe, H.; Kido, J. *Adv. Mater.* **2008**, *20*, 4189−4194. (b) Lyu, Y.-Y.; Kwak, J.; Jeon, W. S.; Byun, Y.; Lee, H. S.; Kim, D.; Lee, C.; Char, K. *Adv. Funct. Mater.* **2009**, *19*, 420−427.
(35) Yeh, S.-J.; Wu, M.-F.; Chen, C.-T.; Song, Y.-H.; Chi, Y.; Ho, M.-H.; Hsu, S.-F.; Chen, C. H. *Adv. Mater.* **2005**, *17*, 285−289.
(36) (a) Ma, Y.; Che, C.-M.; Chao, H.-Y.; Zhou, X.; Chan, W.-H.; Shen, J. *Adv. Mater.* **1999**, *11*, 852−857. (b) Yam, V. W.-W.; Chan, C.-L.; Choi, S. W.-K.; Wong, K. M.-C.; Cheng, E. C.-C.; Yu, S.-C.; Ng, P.-K.; Chan, W.-K.; Cheung, K.-K. *Chem. Commun.* **2000**, 53−54. (c) Ma, Y.; Zhou, X.; Shen, J.; Chao, H.-Y.; Che, C.-M. *Appl. Phys. Lett.* **1999**, *74*, 1361−1363.